Polarization-operator approach to optical signatures of axion-like particles in strong laser pulses

S. Villalba-Chávez, T. Podszus, C. Müller

Institut für Theoretische Physik I, Heinrich-Heine-Universität Düsseldorf, Universitätsstr. 1, 40225 Düsseldorf, Germany

arXiv:1612.07952v1 [hep-ph] 23 Dec 2016

Abstract

Hypothetical oscillations of probe photons into axion-like particles might be revealed by exploiting the strong fields of high-intensity laser pulses. Considering an arbitrary plane-wave background, we determine the polarization tensor induced by the quantum fluctuations of the axion field and use it to calculate how the polarimetric properties of an initially linear-polarized probe beam are modified. We find that various experimental setups based on contemporary facilities and instrumentation might lead to new exclusion bounds on the parameter space of these particle candidates. The impact of the pulse shape on the discovery potential is studied via a comparison between the cases in which the wave is modulated by a Gaussian envelope and a $\sin^2$ profile. This analysis shows that the upper limits resulting from the ellipticity are relatively insensitive to this change, whereas those arising from the rotation of the polarization plane turn out to be more dependent on the field shape.

Key words: Beyond the Standard Model, Axion-like particles, Vacuum polarization, Laser Fields.
PACS: 14.80.-j, 12.20.Fv

1. Introduction

A spontaneous breakdown of the global U(1)−Peccei-Quinn symmetry occurs in the course of explaining the absence of charge-parity violation in the theory of strong interactions. The emerging Nambu-Goldstone boson–known as the QCD axion [1–3]–constitutes the flag representative for the axion models [4–7] and the class of Axion-Like Particles (ALPs) that are predicted in conformal scenarios [8], string theory [9–12] as well as various Standard Model extensions, where they are linked to dark matter [13–17]. Despite experimental efforts toward their detection–much of them exploiting their coherent oscillations into photons mediated by a static magnetic field–there is no evidence yet of ALPs. This fact manifests that their interactions with the well established Standard Model branch might be extremely weak, and the absence of positive detection signals can be used to constrict the associated parameter space. Stringent upper bounds on the ALP-diphoton coupling g have been inferred from astrophysical considerations. A plausible generation of ALPs in the core of stars via the Primakoff process might lead to an energy loss which accelerates their cooling and, therefore, their lifetimes. The nonobservation of a diminishing in the number of stars in the Helium-burning phase [horizontal-branch (HB) stars] within globular clusters constraints g to lie below $g \lesssim 10^{-10}$ GeV^{-1} for ALP masses m below the keV scale [18–20]. Furthermore, as these particle candidates may escape from the Sun almost freely, solar ALPs would likely arrive to Earth. By monitoring these hypothetical ALP fluxes, the CAST collaboration has obtained $g < 9 \times 10^{-11}$ GeV^{-1}, whenever m is below 10 meV [21, 22].

Bounds resulting from laboratory experiments are considerably less stringent but free from the uncertainty associated with the underlying astrophysical models [23–26]. Some of them have been established from the search of Light Shining through a Wall (LSW) [27–34] and from scenarios oriented to detect the magnetically-induced vacuum dichroism and birefringence mediated by real and virtual ALPs, respectively [35–40]. While in LSW setups, the best upper limit is held by the OSCAR collaboration $g < 4 \times 10^{-8}$ GeV^{-1} [34], the current best bound resulting from polarimetric studies has been established by PVLAS $g < 8 \times 10^{-8}$ GeV^{-1} [40]. These limits apply for $m \lesssim 100\,\mu$eV, and relax significantly for masses larger than $m > 10$ meV by several orders of magnitude. As a general feature both, LSW and polarimetric setups, might improve their respective bounds by increasing the field strength and the distance over which it extends. At present, the largest magnetic field generated by superconducting dipole magnets amounts to $\sim 10^6$ G over a length smaller than 10 m. The incorporation of interferometric cavities for the probe beam allows for extending the interaction region upto five orders of magnitude, but its use has not been enough to push down the bounds in regions of masses $m > 10$ meV, where they turn out to be much less stringent.

Higher field strengths $\sim 10^9$ G can be obtained nowadays within the focal spots of high-intensity laser pulses. Even larger magnetic fields $\sim 10^{11}$ G, i.e. two orders of magnitude below the critical scale $B_c = 4.42 \times 10^{13}$ G of Quantum Electrodynamics (QED), are envisaged in the near future within the ELI and XCELS projects [41, 42]. Despite the inhomo-

Email addresses: selym@tp1.uni-duesseldorf.de (S. Villalba-Chávez), tobias.podszus@hhu.de (T. Podszus), c.mueller@tp1.uni-duesseldorf.de (C. Müller)

geneous nature of these pulses–confined to short spatial extensions $\sim \mu$m–their use may allow for the realization of various elusive QED processes [43]. For instance, the HIBEF collaboration [44, 45] has put forward a laser-based experiment with which vacuum birefringence [46–49] may soon be detected. This kind of experiment provides propitious arenas to test the frontier of the Standard Model at low energies [50–53] and therefore, complements those setups driven by particle accelerators. Various theoretical studies in this direction have been carried out to estimate whether high-intensity laser pulses are feasible in the searches for ALPs [54–59], minicharged particles and hidden photons [60–63]. However, the complicated nature of pulsed laser fields makes the phenomenological descriptions rather challenging and full characterizations of these problems are far from being complete.

In this Letter, we provide a step toward the understanding of the role that the pulse profile may play in the search for ALPs, this way extending a recent investigation carried out within the context of minicharged particles [63]. We show that, when dealing with a polarimetric probe driven by the field of a high-intensity linearly polarized pulse, the upper limits resulting from the ellipticity are almost insensitive to the pulse shape, whereas those arising from the rotation of the polarization plane turn out to be more dependent on the field profile. Besides, we reveal that this kind of setup might notably improve the existing laboratory limits in some regions of the ALP parameter space. Our investigation relies on the polarization tensor induced by the quantum fluctuations of the axion field over a plane-wave background.

2. Photon propagation in the vacuum of ALPs

Searches for axion dark matter rely on the existence of an ALPs background permeating the universe. In the following we will assume that the effects resulting from this nontrivial expectation value are negligible in comparison with the quantum fluctuations that are induced by a pseudoscalar field $\phi(x)$ on the propagation of a small-amplitude electromagnetic wave $a_\mu(x)$. We are interested in evaluating these effects in an external electromagnetic field characterized by the tensor $\mathscr{F}^{\mu\nu} = \partial^\mu \mathscr{A}^\nu - \partial^\nu \mathscr{A}^\mu$ with $\mathscr{A}_\mu(x)$ denoting its four-potential. As long as the fields of interest are minimally coupled, preserving the formal invariance properties of QED, the relevant equations of motion are[1]

$$\begin{aligned} &\Box a^\mu(x) + g\tilde{\mathscr{F}}^{\mu\nu}(x)\partial_\nu\phi(x) = 0, \\ &\left(\Box + m^2\right)\phi(x) - \frac{1}{8\pi} g\tilde{\mathscr{F}}^{\mu\nu}(x) f_{\mu\nu}(x) = 0, \end{aligned} \tag{1}$$

provided that $a_\mu(x)$ is chosen in the Lorenz gauge $\partial_\mu a^\mu = 0$ and $\Box \equiv \partial_\mu\partial^\mu = \partial^2/\partial t^2 - \nabla^2$. Here the coupling constant g and mass m are unknown parameters, $f^{\mu\nu} = \partial^\mu a^\nu - \partial^\nu a^\mu$, whereas the dual of the external field tensor is $\tilde{\mathscr{F}}^{\mu\nu} = \frac{1}{2}\epsilon^{\mu\nu\alpha\beta}\mathscr{F}_{\alpha\beta}$. When solving the second equation involved in (1) and substituting the expression for $\phi(x) = \frac{g}{8\pi(\Box+m^2)}\tilde{\mathscr{F}}^{\mu\nu}(x) f_{\mu\nu}(x)$ into the equation associated with the small-amplitude wave, we end up with

$$\begin{aligned} &\Box a^\mu(x) + \int d^4\tilde{x}\, \Pi^{\mu\nu}(x,\tilde{x}) a_\nu(\tilde{x}) = 0, \\ &\Pi^{\mu\nu}(x,\tilde{x}) = -\frac{ig^2}{4\pi}\tilde{\mathscr{F}}^{\mu\tau}(x)\left[\partial^x_\tau\partial^{\tilde{x}}_\sigma \Delta_{\rm F}(x-\tilde{x})\right]\tilde{\mathscr{F}}^{\sigma\nu}(\tilde{x}), \end{aligned} \tag{2}$$

where $\Delta_{\rm F}(x-\tilde{x}) = \int \frac{d^4p}{(2\pi)^4}\frac{i}{p^2-m^2+i0}e^{-ip(x-\tilde{x})}$ denotes the ALP propagator. Note that Eq. (2) has been written in a way that resembles the effective equation of motion of the electromagnetic field in QED, i.e., including the photon radiative correction. This fact allows us to identify straightforwardly the polarization tensor $\Pi^{\mu\nu}(x,\tilde{x})$ induced by the quantum vacuum fluctuations of the pseudoscalar field $\phi(x)$. The Feynman diagram associated with this tensor is depicted in Fig. 1.

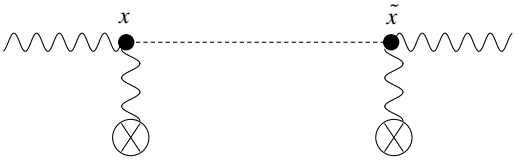

Figure 1: Diagrammatic representation of the vacuum polarization tensor mediated by a quantum fluctuation of a pseudoscalar field $\phi(x)$ in a high-intensity laser pulse [vertical wavy lines]. Here, the dashed line represents the ALP propagator $\Delta_{\rm F}(x,\tilde{x})$, whereas the horizontal wavy lines must be understood as the amputated photon legs.

Hereafter, we indentify the background described by $\mathscr{F}^{\mu\nu}(x)$ with the field produced by a high-intensity laser, the potential of which is taken in the form

$$\mathscr{A}^\mu(x) = a_1^\mu\psi_1(\varphi) + a_2^\mu\psi_2(\varphi), \tag{3}$$

where $a_{1,2}$ are two orthogonal amplitude vectors [$a_1 a_2 = 0$] and $\psi_{1,2}(\varphi)$ arbitrary functions of $\varphi = \varkappa x$ satisfying the boundary conditions $\psi_{1,2}(\pm\infty) = \psi'_{1,2}(\pm\infty) = 0$. Here, the prime denotes the derivative with respect to the argument, $\psi'_{1,2}(\varphi) \equiv d\psi_{1,2}(\varphi)/d\varphi$. The external potential is chosen in the Lorenz gauge $\partial_\mu\mathscr{A}^\mu = 0$ so that the wave four-vector $\varkappa^\mu = (\varkappa^0, \boldsymbol{\varkappa})$ with $\varkappa^2 = 0$ and the amplitude vectors $a^\mu_{1,2}$ satisfy the constraints $\varkappa a_{1,2} = 0$. The presence of this plane-wave background allows for introducing the four-vectors

$$\Lambda^\mu_{1,2}(q) = -\frac{\mathscr{F}^{\mu\nu}_{1,2}q_\nu}{q\varkappa\sqrt{-a^2_{1,2}}}, \quad \tilde{\Lambda}^\mu_{1,2}(q) = -\frac{\tilde{\mathscr{F}}^{\mu\nu}_{1,2}q_\nu}{q\varkappa\sqrt{-a^2_{1,2}}}, \tag{4}$$

which are built up from the amplitudes of the external field modes $\mathscr{F}^{\mu\nu}_i = \varkappa^\mu a^\nu_i - \varkappa^\nu a^\mu_i$ [$i = 1, 2$]. These vectors are transverse $q_\mu\Lambda^\mu_{1,2}(q) = q_\mu\tilde{\Lambda}^\mu_{1,2}(q) = 0$, orthonormalized according to $\Lambda^\mu_i(q)\Lambda_{j\mu}(q) = \tilde{\Lambda}^\mu_i(q)\tilde{\Lambda}_{j\mu}(q) = -\delta_{ij}$ and satisfy the relation $\tilde{\Lambda}^\mu_i(q)\Lambda_{j\mu}(q) = -\epsilon_{ij}$ with $i, j = 1, 2$. Here the antisymmetric tensor ϵ_{ij} with $\epsilon_{12} = 1$ is used.

In the following, we Fourier transform Eq. (2) and seek the solutions of the resulting equation of motion in the form of a su-

[1] From now on "natural" and Gaussian units $c = \hbar = 4\pi\epsilon_0 = 1$ are used. Besides, the metric tensor $g_{\mu\nu}$ is taken with signature $(+1, -1, -1, -1)$ so that $\mathcal{A}\mathcal{B} = \mathcal{A}_0\mathcal{B}_0 - \boldsymbol{\mathcal{A}}\cdot\boldsymbol{\mathcal{B}}$.

perposition of transverse waves $a^\mu(q) = \sum_{i=1,2} \Lambda_i^\mu(q) f_i(q)$. Correspondingly,

$$
\begin{aligned}
q_2^2 f_i(q_2) &= -\sum_j \int \frac{d^4q_1}{(2\pi)^4} \Lambda_j^\mu(q_1) \Pi_{\mu\nu}(q_1, q_2) \Lambda_i^\nu(q_2) f_j(q_1), \\
\Pi_{\mu\nu}(q_1, q_2) &= \int d^4x\, d^4\tilde{x}\, e^{-iq_1 x} \Pi_{\mu\nu}(x, \tilde{x}) e^{iq_2 \tilde{x}}.
\end{aligned}
\tag{5}
$$

In obtaining the expression above we have used the symmetry property $\Pi_{\mu\nu}(-q_2, -q_1) = \Pi_{\nu\mu}(q_1, q_2)$. From now on, we choose the reference frame in such a way that the direction of propagation of our external plane wave [see Eq. (3)] is along the positive direction of the third axis. As a consequence, the external field only depends on $x_- = (x^0 - x^3)/\sqrt{2}$ via $\varphi = \varkappa_+ x_-$ with $\varkappa_+ = (\varkappa^0 + \varkappa^3)/\sqrt{2} = \sqrt{2}\varkappa_0 > 0$.

Next, we insert the polarization tensor in position space [see Eq. (2)] into Eq. (5). Afterwards, integrations by parts over x and $\tilde{x}$ are carried out considering the boundary condition $\psi'_{1,2}(\pm\infty) = 0$. Later, we introduce the light-cone variables $x_\pm = (x^0 \pm x^3)/\sqrt{2}$, $\boldsymbol{x}_\perp = (x^1, x^2)$ and $\tilde{x}_\pm = (\tilde{x}^0 \pm \tilde{x}^3)/\sqrt{2}$, $\tilde{\boldsymbol{x}}_\perp = (\tilde{x}^1, \tilde{x}^2)$. Their use allows us to integrate six out of the eight variables involved in $\Pi^{\mu\nu}(q_1, q_2)$. As a consequence,

$$
\Pi^{\mu\nu}(q_1, q_2) = \frac{\delta_{q_2, q_1}}{\varkappa_+} \int d\tilde{\varphi}\, \mathcal{P}^{\mu\nu}(\tilde{\varphi}, q_1, q_2) e^{\frac{iq_{2+}}{\varkappa_+}\tilde{\varphi}},
\tag{6}
$$

where the notation $\delta_{q_2,q_1} = (2\pi)^3 \delta^{(\perp)}(q_2 - q_1)\delta^{(-)}(q_2 - q_1)$ has been introduced. The tensorial structure of $\mathcal{P}^{\mu\nu}(\tilde{\varphi}, q_1, q_2)$ resembles the one associated with the polarization tensor of QED [63]:

$$
\begin{aligned}
\mathcal{P}^{\mu\nu}(\tilde{\varphi}, q_1, q_2) = {} & c_1 \Lambda_1^\mu(q_1)\Lambda_2^\nu(q_2) + c_2 \Lambda_2^\mu(q_1)\Lambda_1^\nu(q_2) \\
& + c_3 \Lambda_1^\mu(q_1)\Lambda_1^\nu(q_2) + c_4 \Lambda_2^\mu(q_1)\Lambda_2^\nu(q_2).
\end{aligned}
\tag{7}
$$

As $q_1 - q_2 \sim \varkappa$, this decomposition does not depend on which choice of q is taken; see also Eq. (4). The involved form factors c_i depend on the phase of the external field $\tilde{\varphi}$, q_1 and q_2. Explicitly,

$$
\begin{aligned}
c_1 &= \frac{g^2}{2\varkappa_0^2}(\varkappa q_2)\sqrt{I_1 I_2} \int \frac{d\eta}{2\pi} \frac{\tilde{\psi}_2(\eta_{q_1})\psi'_1(\tilde{\varphi})}{\eta - \frac{q_{1\perp}^2 + m^2}{2\varkappa q_1} + i0} e^{-i\eta\tilde{\varphi}}, \\
c_3 &= -\frac{g^2}{2\varkappa_0^2}(\varkappa q_2) I_2 \int \frac{d\eta}{2\pi} \frac{\tilde{\psi}_2(\eta_{q_1})\psi'_2(\tilde{\varphi})}{\eta - \frac{q_{1\perp}^2 + m^2}{2\varkappa q_1} + i0} e^{-i\eta\tilde{\varphi}}, \\
c_2 &= c_1(1 \leftrightarrow 2), \quad c_4 = c_3(1 \leftrightarrow 2),
\end{aligned}
\tag{8}
$$

where $\eta_{q_1} \equiv \eta - (q_1^2 + q_{1\perp}^2)/(2\varkappa q_1)$ and the change of variable $\eta = -p_+/\varkappa_+$ has been carried out. In Eq. (8), the exchange $1 \leftrightarrow 2$ must be carried out only on the index of the field profile functions $\psi'_{1,2}$ and on the peak intensity associated with each external field mode $I_{1,2} = E_{1,2}^2/(4\pi)$ with $E_{1,2}^2 = -\varkappa_0^2 a_{1,2}^2$. Here $\tilde{\psi}_{1,2}(\alpha) = \int d\varphi\, \psi'_{1,2}(\varphi) e^{i\alpha\varphi}$ is the Fourier transform of $\psi'_{1,2}(\varphi)$. We remark that also other representations for c_i can be found. We will see, however, that the chosen one turns out to be convenient for the purposes of this work.

We solve Eq. (2) by following a procedure similar to the one used in the context of minicharged particles [see Ref. [63]]. If the ALP effects do not modify the Maxwell equations dramatically, one can solve Eq. (5) perturbatively by setting $f_i(q) \approx f_{0i}(q) + \delta f_i(q)$. In the following, we suppose a head-on collision between the strong laser pulse and the probe beam characterized by a four-momentum $k^\mu = (\omega_{\boldsymbol{k}}, \boldsymbol{k})$, so that $\varkappa_+ k_- = 2\omega_{\boldsymbol{k}}\varkappa_0$ and $\boldsymbol{k}_\perp = \boldsymbol{0}$. In accordance, the leading order term is $f_{0i}(q) = |2q_-|a_{0i}(2\pi)^4\delta(q^2)\,\delta^{(\perp)}(q)\,\delta^{(-)}(q-k)$, corresponding to $f_{0i}(x) = a_{0i}e^{-i\phi}$ with $\phi = kx = k_- x_+$ and a_{0i} the amplitude of mode-i. Besides, it follows from Eq. (5) that the perturbative contribution is given by

$$
\begin{aligned}
\delta f_i(q_2) = {} & -\frac{\delta_{q_2,k}}{\varkappa_+\left[2q_{2+}q_{2-} - q_{2\perp}^2 + i0\right]} \sum_j a_{0j} \int d\tilde{\varphi} \\
& \times \Lambda_j^\mu(k)\mathcal{P}_{\mu\nu}(\tilde{\varphi}, k, q_2)\Lambda_i^\nu(q_2) e^{\frac{iq_{2+}}{\varkappa_+}\tilde{\varphi}},
\end{aligned}
\tag{9}
$$

where it must be understood that the only nonvanishing light-cone component of the four-vector k^μ is k_-. Besides, the poles in the function $1/q_2^2$ have been shifted infinitesimally into the complex plane by an $i0$-term so that correct boundary conditions of the fields at asymptotic times $f_i(\pm\infty, \boldsymbol{x})$ are implemented. When Fourier transforming back, the solution of our problem reads $a^\mu(x) = \sum_{i=1,2} \Lambda_i^\mu(k) f_i(x)$ [see above Eq. (5)], where

$$
\begin{aligned}
f_i(x) \approx e^{-i\phi}\Bigg[& a_{0i} - \frac{1}{2\varkappa_+ k_-} \sum_j a_{0j} \int d\tilde{\varphi} \int \frac{dq_{2+}}{2\pi} \\
& \times \Lambda_j^\mu(k) \frac{\mathcal{P}_{\mu\nu}(\varphi, k, q_2)}{q_{2+} + i0} \Lambda_i^\nu(q_2) e^{\frac{iq_{2+}}{\varkappa_+}(\tilde{\varphi} - \varphi)} \Bigg].
\end{aligned}
\tag{10}
$$

Here, $q_{2-} = k_-$, $\boldsymbol{q}_{2\perp} = \boldsymbol{0}$, whereas $\boldsymbol{k}_\perp = \boldsymbol{0}$ and $k_+ = 0$. We remark that, in our reference frame, the transversality condition $\varkappa a_{1,2} = 0$ [see below Eq. (3)] implies that $a_{1,2-} = 0$. It can be verified that such a constraint implies $\Lambda_{1,2}^\mu(q)$ to be independent of q_+. This means that, in the expression above $\Lambda_i^\nu(q_2) = \Lambda_i^\nu(k)$. Structurally, Eq. (10) coincides with Eq. (8) found in Ref. [63]. This fact allows us to integrate out q_{2+} by using the procedure explained there. As a consequence of this assessment, the integration over $\tilde{\varphi}$ turns out to be restricted to the kinematically allowed region $(-\infty, \varphi]$ and we end up with

$$
\begin{aligned}
f_i(x) \approx {} & f_{0i}(x) \\
& + \frac{i}{2\varkappa_+ k_-} \sum_j f_{0j}(x) \int_{-\infty}^{\varphi} d\tilde{\varphi}\, \Lambda_j^\mu(k)\mathcal{P}_{\mu\nu}(\varphi, k, k)\Lambda_i^\nu(k).
\end{aligned}
\tag{11}
$$

The expression above constitutes the starting point for further considerations. It holds for arbitrary plane-wave profiles, which formally implies that the pulsed field is infinitely extended in the plane perpendicular to the propagation direction. This means that, in our model, ALPs do not experience transverse focusing effects. In an actual experimental realization, this condition can be considered as satisfied whenever the ALP Compton wavelength $\lambda_{\rm ALP} = 1/m$ turns out to be much smaller than the characteristic spatial scale, set by the waist size of the pulse w_0. In order words, the outcomes resulting from Eq. (11) are expected to be trustworthy for ALP masses $m \gg w_0^{-1}$.

When the external plane wave [see Eq. (3)] is linearly polarized with $a_2 = 0$, $\psi_2(\varphi) = 0$, the probe modes in Eq. (11)

disentangle from each other. Consequently, we can write the electric field of the probe [$\boldsymbol{\varepsilon} = -\partial \boldsymbol{a}/\partial x^0$ with $a_0 = 0$] as a superposition of waves

$$\begin{aligned}\boldsymbol{\varepsilon}(x) \approx\ & \varepsilon_0 \cos(\vartheta_0)\boldsymbol{\Lambda}_1 \mathrm{Re}\ \exp\left[-i\phi\right] \\ & + \varepsilon_0 \sin(\vartheta_0)\boldsymbol{\Lambda}_2 \mathrm{Re}\exp\left[-i\phi + \frac{i}{2\varkappa_+ k_-}\int_{-\infty}^{\varphi} d\tilde{\varphi}\ c_4(\tilde{\varphi})\right].\end{aligned} \tag{12}$$

where the approximation $1 + ix \approx \exp(ix)$ has been used. In the expression above only the leading term, which does not vanish at asymptotically large spacetime distances [$\varphi \to \infty$], when the high-intensity laser field is turned off, has been considered. Here ε_0 refers to the initial electric field amplitude, $\boldsymbol{\Lambda}_{1,2} = \boldsymbol{a}_{1,2}/|\boldsymbol{a}_{1,2}|$, whereas $0 \leqslant \vartheta_0 < \pi/2$ is the corresponding initial polarization angle of the probe with respect to $\boldsymbol{\Lambda}_1$, i.e., the polarization axis of the external pulse. In the expression above, the form factor $c_4(\tilde{\varphi})$ [see Eq. (8)] must be evaluated with $q_2 = q_1 = k$. Therefore,

$$\begin{aligned}c_4(\tilde{\varphi}) = & -\frac{g^2}{4\varkappa_0^2}(\varkappa_+ k_-) I_1 \psi_1'(\tilde{\varphi})\frac{1}{\pi}\mathrm{P}\int_{-\infty}^{\infty} d\eta \frac{\tilde{\psi}_1(\eta)e^{-i\eta\tilde{\varphi}}}{\eta - n_*} \\ & + \frac{ig^2}{4\varkappa_0^2}(\varkappa_+ k_-) I_1 \psi_1'(\tilde{\varphi})\,\tilde{\psi}_1(n_*)\, e^{-in_*\tilde{\varphi}},\end{aligned} \tag{13}$$

where the relation $(x+i0)^{-1} = \mathrm{P}\frac{1}{x} - i\pi\delta(x)$, with P refering to the Cauchy principal value, has been applied and $n_* = m^2/(2\varkappa_+ k_-)$ denotes the resonant parameter.

Besides, in this external field configuration, the total probability that a photon with polarization Λ_2 does not decay inside the laser pulse is obtained by evaluating the square of the wave function, $\mathcal{P}_{\gamma\to\gamma}(\varphi) = |\Lambda_2^\mu f_2(\phi,\varphi)|^2/|a_{02}|^2 = 1 - \mathcal{P}_{\gamma\to\phi}(\varphi)$. Here,

$$\mathcal{P}_{\gamma\to\phi}(\varphi) = \frac{g^2 I}{4\varkappa_0^2}\tilde{\psi}_1(n_*)\int_{-\infty}^{\varphi} d\tilde{\varphi}\ \psi_1'(\tilde{\varphi})\, e^{-in_*\tilde{\varphi}} \tag{14}$$

refers to the probability that a photon oscillates into an ALP, a phenomenon which damps the intensity of the probe beam $I(\varphi) = \frac{\varepsilon_0^2}{4\pi}\left[\cos^2(\vartheta_0) + \sin^2(\vartheta_0)\exp(-\kappa)\right]$ as it propagates in the pulse. The factor responsible for the damping is $\kappa(\varphi) \approx \mathcal{P}_{\gamma\to\phi}(\varphi)$, provided $\kappa(\varphi) \ll 1$. Therefore, the vacuum behaves like a dichroic medium, inducing a rotation of the probe polarization from the initial angle ϑ_0 to $\vartheta_0 + \delta\vartheta$, where $\delta\vartheta$ is expected to be tiny. At asymptotically large spacetime distances [$\varphi \to \infty$], we find

$$\begin{aligned}\delta\vartheta(g,m) &\approx -\frac{1}{4}\sin(2\vartheta_0)\mathcal{P}_{\gamma\to\phi}(\infty), \\ \mathcal{P}_{\gamma\to\phi}(\infty) &= \frac{g^2 I}{4\varkappa_0^2}|\tilde{\psi}_1(n_*)|^2.\end{aligned} \tag{15}$$

As the phase difference between the two propagating modes, $\delta\phi(\varphi) = \frac{1}{2\varkappa_+ k_-}\mathrm{Re}\int_{-\infty}^{\varphi} d\tilde{\varphi}\ c_4(\tilde{\varphi})$, does not vanish either, the vacuum is also predicted to be birefringent. Hence, when the strong field is turned off [$\varphi \to \infty$], the outgoing probe should be elliptically polarized and its ellipticity is given by [64]

$$|\psi(g,m)| \approx \frac{1}{2}\sin(2\vartheta_0)\frac{g^2 I}{8\varkappa_0^2}\left|-\frac{1}{\pi}\mathrm{P}\int_{-\infty}^{\infty} d\eta \frac{|\tilde{\psi}_1(\eta)|^2}{\eta - n_*}\right|. \tag{16}$$

We remark that the last formula is a good approximation only when its right-hand side is smaller than unity. Manisfestly, the relation between Eq. (15) and (16) is of Kramers-Kronig type [65].

There exists already significant progress in high-purity polarimetric techniques for x-ray probes [66, 67] which are expected to be exploited in the envisaged experiment at HIBEF [45]. In first instance, the planned polarimeter would be designed to measure vacuum birefringence only. It will involve an analyzer set at a right angle to the initial polarization direction. This is justified because, in a pure QED context with an x-ray probe and an optical strong field, the rotation of the incoming polarization plane is exponentially small [$\delta\vartheta_{\mathrm{QED}} = 0$ for practical purposes]. In accordance, the transmission probability is determined by the ellipticity induced by QED vacuum fluctuations $\mathcal{P} = \psi_{\mathrm{QED}}^2$ only. We remark that isolated detections of both $\delta\vartheta(g,m)$ and $|\psi(g,m)|$ can be carried out if the analyzer is set in such a way that the number of counted photons is minimum. The axis of the analyzer would form an angle $\frac{\pi}{2} + \delta\vartheta(g,m)$ with respect to the initial polarization plane whose measurement allows for establishing $\delta\vartheta(g,m)$. If the minimum count rate differs from zero, this would imply that the outgoing probe beam is elliptically polarized. Therefore, the polarization state transmitted by the analyzer reads $\boldsymbol{e} = \pm\sin(\vartheta_0 + \delta\vartheta)\boldsymbol{\Lambda}_1 \mp \cos(\vartheta_0 + \delta\vartheta)\boldsymbol{\Lambda}_2$. As a consequence, the transmission probability is $\mathcal{P} = |\boldsymbol{e}\cdot\boldsymbol{\varepsilon}|^2/|\varepsilon_0|^2 = \left[\psi_{\mathrm{QED}} + \psi(g,m)\right]^2$. Assuming that $\psi_{\mathrm{QED}} > \psi(g,m)$, we find that the number of photons to be counted reads

$$\mathcal{N} = \mathcal{N}_{\mathrm{in}}\mathcal{N}_{\mathrm{shot}}\mathcal{T}\left[\psi_{\mathrm{QED}}^2 + 2\psi_{\mathrm{QED}}\psi(g,m)\right], \tag{17}$$

where $\mathcal{N}_{\mathrm{shot}}$ counts the number of laser shots used for a measurement, $\mathcal{T}$ denotes the transmission coefficient of all optical components and $\mathcal{N}_{\mathrm{in}}$ is the number of probe photons emitted in each shot. This expression shows that the number of signal photon increases the greater $\psi(g,m)$ is.

3. Consequences of the pulse profile

In this section we particularize the optical obsevables given in Eqs. (15) and (16) for the cases in which the external field is characterized by a Gaussian or a $\sin^2$ envelope [see Fig. 2]. Later, in sec. 3.3, we generalize the results found for these two pulses by considering a generic pulse envelope and a carrier envelope phase (CEP).

3.1. Gaussian pulse

We wish to investigate the optical observables induced by ALPs when the field profile function is of the form

$$\psi_1'(\varphi) = \exp\left[-\frac{(\varphi - \mathcal{N}\pi)^2}{2\Delta\varphi^2}\right]\sin(\varphi). \tag{18}$$

Here $\Delta\varphi = \pi\mathcal{N}/\sqrt{2\ln(2)}$ is defined from the full width at half maximum (FWHM) of the field with $\mathcal{N}$ referring to the number of oscillation cycles within the Gaussian envelope. The Fourier

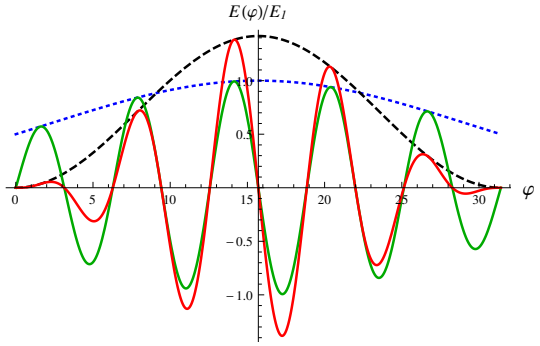

Figure 2: Laser pulses with Gaussian and $\sin^2$-profiles are shown in green and red with $\mathcal{N} = 5$, respectively. While the pure Gaussian envelope is dotted in blue, the one associated with the $\sin^2$ function is dashed in black. These envelopes are given as references. As the $\sin^2$ −pulse falls off faster than the Gaussian pulse, its peak strength must be higher ir order to contain the same total energy.

transform of this pulse allows us to express the rotation angle [see Eq. (15)] in the following form

$$\begin{aligned}\delta\vartheta(g,m) &\approx -\frac{1}{4}\sin(2\vartheta_0)\mathcal{P}_{\gamma\to\phi},\\ \mathcal{P}_{\gamma\to\phi} &= \frac{\pi}{2}\frac{g^2}{\varkappa_0^2} I\Delta\varphi^2 e^{-\Delta\varphi^2(n_*^2+1)}\sinh^2\left(\Delta\varphi^2 n_*\right).\end{aligned} \tag{19}$$

Assuming the condition $\Delta\varphi^2 > \Delta\varphi^2 n_* \gg 1$, one can use the approximation $\sinh^2(\Delta\varphi^2 n_*) \approx \frac{1}{4}\exp[2\Delta\varphi^2 n_*]$. Its substitution into Eq. (19) leads to

$$\delta\vartheta(g,m) \approx -\frac{1}{4}\sin(2\vartheta_0)\frac{\pi}{8}\frac{g^2}{\varkappa_0^2} I\Delta\varphi^2 e^{-\Delta\varphi^2(n_*-1)^2}. \tag{20}$$

Since the rotation angle is maximized in the vicinity of $n_* = m^2/(2\varkappa_+ k_-) \approx 1$, we can anticipate that the most stringent bound will arise at the resonant mass $m_* \equiv \sqrt{2(\varkappa_+ k_-)}$. On the other hand, since $\Delta\varphi^2 n_* \ll 1 < \Delta\varphi^2$ implies $\sinh(\Delta\varphi^2 n_*) \approx \Delta\varphi^2 n_*$ [see Eq. (19)], we find that $|\delta\vartheta(g,m)| \sim n_*^2\Delta\varphi^6\exp(-\Delta\varphi^2)$ is exponentially suppressed, which indicates that in this regime vacuum dichroism tends to vanish.

The ellipticity [see Eq. (16)] can be determined straightforwardly by noting that the Hilbert transform of a Gaussian function $\frac{1}{\pi}\mathrm{P}\int_{-\infty}^{\infty} dz \frac{e^{-z^2}}{y-z} = \frac{2}{\sqrt{\pi}}\mathcal{D}_F(y)$ is specified by the Dawson integral $\mathcal{D}_F(y) = e^{-y^2}\int_0^y dz\, e^{z^2}$ [69]. With this detail in mind, we find

$$\begin{aligned}|\psi(g,m)| \approx \frac{1}{2}\sin(2\vartheta_0)\frac{\sqrt{\pi}}{8}\frac{g^2}{\varkappa_0^2} I\Delta\varphi^2\Big|&\mathcal{D}_F\left(\Delta\varphi\left[1+n_*\right]\right)\\ &- \mathcal{D}_F\left(\Delta\varphi\left[1-n_*\right]\right) - 2e^{-\Delta\varphi^2}\mathcal{D}_F(\Delta\varphi n_*)\Big|.\end{aligned} \tag{21}$$

Let us consider the asymptotic behavior of $|\psi(g,m)|$ as $1 \ll n_*$. Then, $\mathcal{D}_F(\Delta\varphi(1\pm n_*)) \approx \pm\mathcal{D}_F(\Delta\varphi n_*)$, and

$$\begin{aligned}|\psi(g,m)| \approx \frac{1}{2}\sin(2\vartheta_0)\frac{\sqrt{\pi}}{4}\frac{g^2}{\varkappa_0^2} I\Delta\varphi^2\\ \times\left|\mathcal{D}_F\left(\Delta\varphi n_*\right)\right|\left[1-e^{-\Delta\varphi^2}\right].\end{aligned} \tag{22}$$

If $\Delta\varphi n_* \gg 1$, we can use $\mathcal{D}_F(y) \approx 1/(2y) - 1/(4y^3)$ and find that $|\psi(g,m)| \approx \frac{1}{2}\sin(2\vartheta_0)\sqrt{\pi}g^2 I\Delta\varphi/[8\varkappa_0^2 n_*]$.

Turning our attention to the situation in which $n_* \ll 1$, the resulting expression for the ellipticity in this limit reads

$$\begin{aligned}|\psi(g,m)| \approx \frac{1}{2}\sin(2\vartheta_0)\frac{\sqrt{\pi}}{4}\frac{g^2}{\varkappa_0^2} I\Delta\varphi^3 n_*\Big|&1 - 2\Delta\varphi\mathcal{D}_F(\Delta\varphi)\\ &- e^{-\Delta\varphi^2}\frac{\mathcal{D}_F\left(\Delta\varphi n_*\right)}{\Delta\varphi n_*}\Big|,\end{aligned} \tag{23}$$

where the defining equation of the Dawson function has been used, $\mathcal{D}_F'(\Delta\varphi) = 1 - 2\Delta\varphi\mathcal{D}_F(\Delta\varphi)$. The last factor in Eq. (23), i.e. $\mathcal{D}_F\left(\Delta\varphi n_*\right)/(\Delta\varphi n_*) \sim 1$ as $\Delta\varphi n_* \ll 1$. Conversely, the case $\Delta\varphi n_* \gg 1$ can be investigated through $\mathcal{D}_F(\Delta\varphi) \approx \frac{1}{2\Delta\varphi} - \frac{1}{4\Delta\varphi^3}$, in which case the induced ellipticity reads $|\psi(g,m)| \approx \frac{1}{2}\sin(2\vartheta_0)\sqrt{\pi}g^2 I\Delta\varphi n_*/[8\varkappa_0^2]$. The behavior of the ellipticity in a vicinity of the resonance $n_* \approx 1$ is also of interest. In such a case, Eq. (21) reduces to

$$\begin{aligned}\lim_{m\to m_*}|\psi(g,m)| \approx \frac{1}{2}\sin(2\vartheta_0)\frac{\sqrt{\pi}}{8}\frac{g^2}{\varkappa_0^2} I\Delta\varphi^2\\ \times\left|\mathcal{D}_F\left(2\Delta\varphi\right) - 2e^{-\Delta\varphi^2}\mathcal{D}_F(\Delta\varphi)\right|.\end{aligned} \tag{24}$$

For $\Delta\varphi \gg 1$, it leads to $|\psi(g,m_*)| \approx \sin(2\vartheta_0)\sqrt{\pi}g^2 I\Delta\varphi/[64\varkappa_0^2]$.

3.2. $\sin^2$ −*pulse*

In order to evaluate the extent to which the projected bounds might depend on the pulse profile, we will now consider the case in which the function $\psi_1'(\varphi)$ is of the form

$$\begin{aligned}\psi_1'(\varphi) &= \mathcal{R}\sin^2\left[\varphi/(2\mathcal{N})\right]\sin(\varphi)\\ &= \frac{1}{2}\mathcal{R}\sin(\varphi) - \frac{1}{4}\mathcal{R}\sin(\lambda_+\varphi) - \frac{1}{4}\mathcal{R}\sin(\lambda_-\varphi)\end{aligned} \tag{25}$$

for $\varphi \in [0, 2\pi\mathcal{N}]$ and zero otherwise. As before, $\mathcal{N} > 1$ denotes the number of oscillation cycles within the $\sin^2$ −envelope and $\lambda_\pm = 1 \pm \mathcal{N}^{-1}$. The scaling parameter $\mathcal{R}^2 \approx \frac{2}{3}\sqrt{\frac{2\pi}{\ln(2)}}$ is chosen in such a way that the total energy of the pulse coincides with the one of the Gaussian pulse.

The use of the Fourier transform of Eq. (25) allows us to express the rotation angle [see Eq. (15)] in the following form

$$\begin{aligned}\delta\vartheta(g,m) \approx -\frac{1}{4}\sin(2\vartheta_0)\frac{g^2}{4\varkappa_0^2}\mathcal{R}^2 I\sin^2\left(\pi n_*\mathcal{N}\right)\\ \times\left[\frac{1}{n_*^2-1} - \frac{\lambda_+}{2(n_*^2-\lambda_+^2)} - \frac{\lambda_-}{2(n_*^2-\lambda_-^2)}\right]^2.\end{aligned} \tag{26}$$

This expression is characterized by three resonances: $n_* = 1$ and $n_* = \lambda_\pm$. While the former is already known from the analysis of the previous case [see below Eq. (20)], the remaining ones define two additional resonant masses $m_{*\pm} = \sqrt{2\lambda_\pm\varkappa_+ k_-}$ which do not emerge in the framework of the Gaussian pulse. These extra resonances are direct consequences of the side-band terms arising in the spectral decomposition of the $\sin^2$ −pulse, i.e.

the last two contributions in the second line in Eq. (25). We note that the behavior of $\delta\vartheta(g,m)$ when $\pi\mathcal{N}(n_*-1)\ll 1$ or $\pi\mathcal{N}(n_*-\lambda_\pm)\ll 1$, i.e., in a vicinity of m_* and $m_{*\pm}$ is given, respectively, by

$$\delta\vartheta(g,m)\approx -\frac{1}{4}\sin(2\vartheta_0)\frac{g^2\mathcal{R}^2 I}{64\varkappa_0^2}\pi^2\mathcal{N}^2\left\{\begin{array}{ll}4 & \text{for } m\approx m_*\\ 1 & \text{for } m\approx m_{*\pm}\end{array}\right. \tag{27}$$

Comparing the first line of this result with the outcome resulting from Eq. (20) we find that the projected sensitivity expected from a $\sin^2-$pulse will be smaller than the one corresponding to a Gaussian profile by a factor $8/(9\mathcal{R}^2)\approx 0.4$, approximately. Observe that Eq. (26) tends to vanish as $n_*\gg\lambda_+$ and $n_*\ll\lambda_-$. Hence, far from the resonant mass m_* the projected bounds to be determined from the rotation angle are expected to be less stringent.

Now we focus on the ellipticity [see Eq. (16)]. In this case, it is convenient to use the Hilbert transforms $\frac{1}{\pi}\mathrm{P}\int_{-\infty}^{\infty}\frac{dz\sin^2(z)}{(y-z)z^2}=\frac{1}{y}-\frac{\sin(2y)}{2y^2}$ and $\frac{1}{\pi}\mathrm{P}\int_{-\infty}^{\infty}\frac{dz\sin^2(z)}{(y-z)z}=-\frac{\sin(2y)}{2y}$ with which we obtain

$$\begin{aligned}|\psi(g,m)|\approx\frac{1}{2}\sin(2\vartheta_0)\frac{g^2\mathcal{R}^2 I\pi n_*\mathcal{N}}{16\varkappa_0^2}\Bigg|&\frac{1}{n_*^2-1}\\&+\frac{1}{4(n_*^2-\lambda_+^2)}+\frac{1}{4(n_*^2-\lambda_-^2)}-\frac{\sin(2\pi n_*\mathcal{N})}{\pi n_*\mathcal{N}}\\&\times\left[\frac{1}{n_*^2-1}-\frac{\lambda_+}{2(n_*^2-\lambda_+^2)}-\frac{\lambda_-}{2(n_*^2-\lambda_-^2)}\right]^2\Bigg|.\end{aligned} \tag{28}$$

Observe that $|\psi(g,m)|\to 0$ as $n_*\gg\lambda_+$ and $n_*\ll\lambda_-$, whereas for $n_*-1\ll(2\pi\mathcal{N})^{-1}$ we obtain

$$|\psi(g,m)|\approx\frac{1}{2}\sin(2\vartheta_0)\frac{g^2\mathcal{R}^2 I\pi\mathcal{N}}{64\varkappa_0^2}\left|\frac{4\lambda_++1}{1-\lambda_+^2}+\frac{4\lambda_-+1}{1-\lambda_-^2}\right|. \tag{29}$$

We point out that, for $\mathcal{N}\gg 1$, the expression above coincides with the corresponding outcome resulting from a Gaussian pulse [see below Eq. (24)].

3.3. Generalization: $f(\varphi)$-pulse

The laser pulses discussed in the previous sections can be understood as particular cases of a more general situation in which the profile function is given by

$$\psi_1'(\varphi)=\mathcal{R}f(\varphi)\cos(\varphi+\varphi_{\mathrm{CEP}}). \tag{30}$$

Here, $f(\varphi)$ with $f(\varphi)>0$ and $f(\pm\infty)=0$ is a real analytic function in the upper half plane which is maximized at $\varphi=\pi\mathcal{N}$, whereas φ_{CEP} is the CEP. As before, the scaling parameter:

$$\mathcal{R}^2=\frac{\sqrt{\pi}\Delta\varphi\left(1-e^{-\Delta\varphi^2}\cos(\pi\mathcal{N})\right)}{2\int_{-\infty}^{\infty}dx^3 f^2(\varphi)\cos^2(\varphi+\varphi_{\mathrm{CEP}})}, \tag{31}$$

guarantees that the pulse energy is invariant with respect to the chosen profile. Moreover, it must be understood that $\mathcal{R}^2$ does not depend on time and an explicit evaluation of it can be done by setting $x^0=0$. In this context, the angle rotated by the polarization plane [see Eq. (15)]

$$\begin{aligned}\delta\vartheta(g,m)&\approx-\frac{1}{4}\sin(2\vartheta_0)\mathcal{P}_{\gamma\to\phi}(\infty),\\ \mathcal{P}_{\gamma\to\phi}(\infty)&=\frac{g^2 I\mathcal{R}^2}{16\varkappa_0^2}|\tilde{f}(n_*+1)+\tilde{f}(n_*-1)e^{-2i\varphi_{\mathrm{CEP}}}|^2\end{aligned} \tag{32}$$

coincides with an outcome obtained in Ref. [57] upto the scaling factor $\mathcal{R}^2$. There, this formula was established by computing $\mathcal{P}_{\gamma\to\phi}(\infty)$ via the S-matrix element associated with the photon-ALP oscillations and by exploiting the relation between this quantity and the absorption coefficient [see discussion above Eq. (15)]. The equivalence between both procedures is expected because the optical theorem establishes that $\mathcal{P}_{\gamma\to\phi}(\infty)$ is determined by the imaginary part of the vacuum polarization tensor depicted in Fig. 1.

We should however indicate that, in the aforementioned reference, the corresponding expression for the ellipticity was not derived. According to Eq. (16), this observable reads

$$\begin{aligned}|\psi(g,m)|\approx\frac{1}{2}\sin(2\vartheta_0)\frac{g^2 I\mathcal{R}^2}{32\varkappa_0^2}\Bigg|&-\frac{1}{\pi}\mathrm{P}\int_{-\infty}^{\infty}\frac{d\eta}{\eta-n_*}\\&\times|\tilde{f}(\eta+1)+\tilde{f}(\eta-1)e^{-2i\varphi_{\mathrm{CEP}}}|^2\Bigg|.\end{aligned} \tag{33}$$

In these formulae, $\tilde{f}(\alpha)=\int d\varphi f(\varphi)e^{i\alpha\varphi}$ is the Fourier transform of the shape function $f(\varphi)$. The presence of $\tilde{f}(n_*\pm 1)$ in Eqs. (32) and (33) manifests that the projected exclusion regions will depend on the envelope function of the external laser pulse. Besides, these formulae indicate that the CEP allows for interference between the $\tilde{f}(n_*+1)$ and $\tilde{f}(n_*-1)$ terms whenever $\varphi_{\mathrm{CEP}}\neq(2\mathcal{K}+1)\pi/2$ and $\mathcal{K}\in\mathbb{Z}$. This interference effect may be constructive or destructive, depending on the overall sign of the associated contribution. Therefore, an appropriate choice of the CEP may help to optimize the optical signals. For the pulses analyzed previously [see Eqs. (18) and (25)], this occurs for $\varphi_{\mathrm{CEP}}=2\mathcal{K}\pi$ with $\mathcal{K}\in\mathbb{Z}$.

4. Experimental prospects

First we estimate the projected limits considering the benchmark parameters of the proposed experiment at HIBEF [45]. In this setup the strong field will be produced by a Petawatt laser operating in the optical regime with $\varkappa_0\approx 1.55$ eV [$\lambda_0=800$ nm], a repetition rate of 1 Hz, a temporal pulse length of about 30 fs [$\Delta\varphi\approx 11\pi$], and a peak intensity $I\approx 2\times 10^{22}$ W/cm^2. The envisaged probe beam is the European x-ray free electron laser, operating with frequency $\omega_{\boldsymbol{k}}=12.9$ keV and delivering $\mathcal{N}_{\mathrm{in}}\approx 5\times 10^{12}$ photons per shot. The transmission coefficient of the optics to be used in this experiment is $\mathcal{T}=0.0365$, and the incoming polarization angle will be $\vartheta_0=\pi/4$. Under such a conditions, a QED signal as small as $|\psi_{\mathrm{QED}}|=(9.8\pm 6.7)\times 10^{-7}$ rad is likely to be reached provided a perfect overlapping between the probe and the strong laser field is achieved [45].

An exclusion region can be inferred from this projected result by assuming that the induced ellipticity due to ALPs does

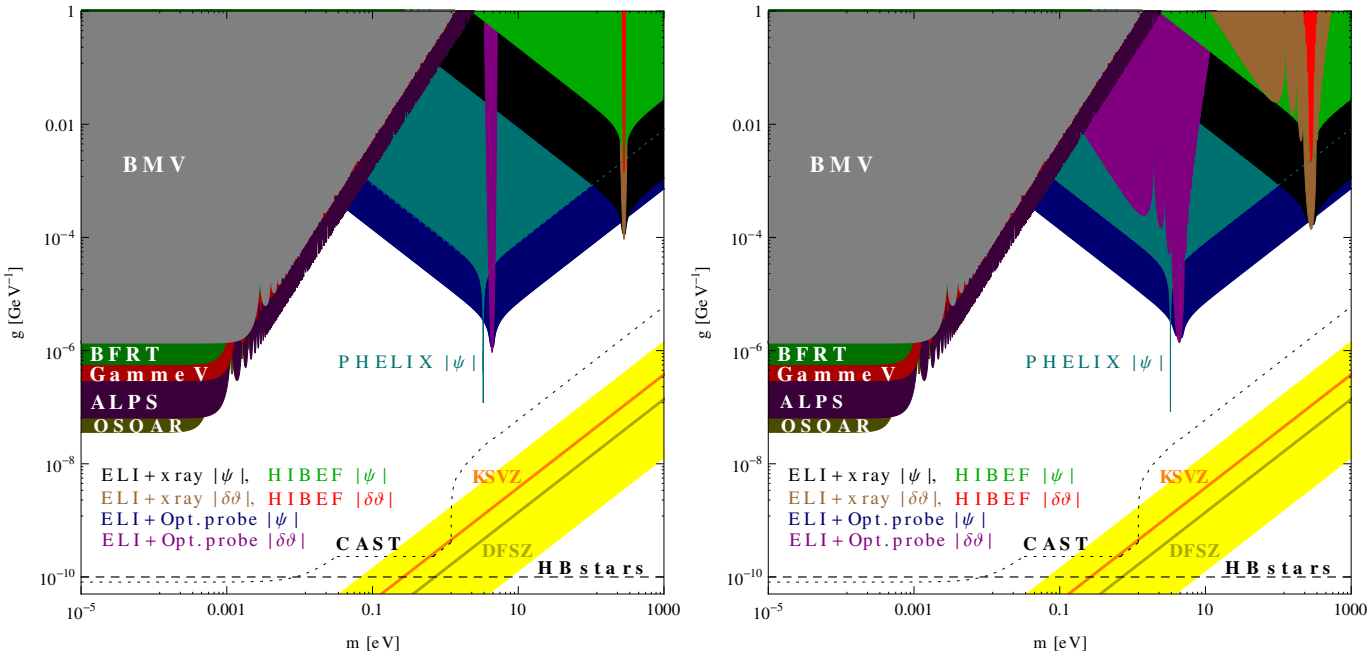

Figure 3: Exclusion regions in the (g, m)-plane obtained from a polarimetric setup driven by an intense linearly polarized laser pulse. The left (right) panel depicts the results based on the Gaussian ($\sin^2$) pulse model. Here the green, black, cyan and blue shaded areas were determined from the ellipticity induced by ALPs on the initial polarization plane Eq. (16), the brown, purple and red wedges were found from the rotation Eq. (15). The respective resonant peaks occur at $m_* = 4.4$ eV [purple] and $m_* = 282.8$ eV [brown, red]. The inclined yellow band covers the predictions of the axion models with $|E/N - 1.95| = 0.07 - 7$ [the notation of this formula is in accordance with Ref. [21]]. The constraints resulting from HB stars [dashed line] are also shown. Further exclusion regions [shaded areas in the upper left corner] provided by different LSW experiment have been included too [see legend]. The exclusion limit resulting from solar monitoring of a plausible ALP flux [CAST experiment] has been included as well [dotted line]. We point out that the upper bound resulting from such an experiment strongly oscillates in the mass region $0.4 \text{ eV} \leqslant m \leqslant 0.6$ eV. This oscillatory pattern has been replaced by a straight dotted line, corresponding to the exclusion limit $g \leqslant 2.3 \times 10^{-10}$ GeV^{-1}, established in [21] at 95% confidence level. For the exact picture of the CAST exclusion limits, we refer the reader to the original publication [21, 22].

not overpass the upper bound set by $|\psi_{\text{QED}}|$. It is shaded in green in the right upper corners in Fig. 3. While the outcome shown in the left panel relies on the Gaussian model, the one in the right panel is based on the $\sin^2$ −pulse. In each panel, there is a tiny wedge shaded in red, which is ruled out by supposing that the rotation angle can be measured with a sensitivity of the same order of magnitude of $|\psi_{\text{QED}}|$. Our estimates reveal that the most stringent bounds $g < 1.4 \times 10^{-3}$ GeV^{-1} [Gaussian profile] and $g < 2.2 \times 10^{-3}$ GeV^{-1} [$\sin^2$ −profile] would emerge at the resonant mass $m_* \approx 282.8$ eV [see below Eq. (20)].

As we already pointed out, the energy scale associated with the waist size of the pulse w_0 limits the validity of our predictions towards smaller ALP masses. In view of the strong focusing applied at HIBEF [$w_0 \approx 2\lambda_0$], our potential discovery applies for $m \gg 0.12$ eV. We must, in addition, mention that this result relies on the forward scattering analysis, and that the waist size of the probe $w_{\text{probe}} = 42.5$ μm is bigger than w_0. This situation in combination with the nonconservation of the transverse momentum that the focusing induces, is favourable to scatter probe photons slightly off the forward direction. Such an effect has been proposed as an alternative way to detect the QED birefringence at a small angle [71]. It might as well be beneficial for the search of ALPs as the signal-to-noise ratio for photons transmitted through the analyzer improves notably. However, this study would require to incorporate the focusing effects, which is still beyond the scope of this work.

If the planned HIBEF experiment was driven by the strong field to be reached at ELI [$I \approx 10^{25}$ W/cm^2, $\varkappa_0 \approx 1.55$ eV, $\tau \approx 13$ fs, corresponding to $\Delta\varphi \approx 4\pi$], and the sensitivity remained within the same order of magnitude $\sim 10^{-6}$, the limits above would be pushed down to $g < 9.3 \times 10^{-5}$ GeV^{-1} [Gaussian model] and $g < 1.4 \times 10^{-4}$ GeV^{-1} [$\sin^2$ −pulse] at the resonant mass $m_* \approx 282.8$ eV. The projected areas to be excluded from the ellipticity [rotation angle] can be seen in Fig. 3 in black [brown]. We emphasize that the pulse at ELI is expected to be strongly focused [$w_0 \sim \lambda_0$]. Hence, the exclusion areas found for this setup are expected to be trustworthy as long as $m \gg 0.24$ eV. Our estimates reveal that the shape of the bounds resulting from the ellipticity almost coincide for both pulse models. However, the borders of the excluded areas coming from the rotation angle differ from each other more strongly.

The described behavior is even more pronounced when both observables are probed with an optical laser beam and the envisaged ELI laser drives the vacuum polarization. The potential exclusion regions associated with this case are summarized in Fig. 3 in blue [ellipticity] and purple [rotation angle]. They have been found by supposing a sensitivity of the order of $\sim 10^{-10}$ rad, a probe frequency $\omega_{\boldsymbol{k}} = 2\varkappa_0 = 3.1$ eV and a probe intensity much smaller than the one of the strong laser field. We remark that the outcomes resulting from this hypothetical setup were obtained by considering a counterpropagating geometry

$\varkappa_+ k_- = 2\varkappa_0 \omega_{\boldsymbol{k}}$ and an initial polarization angle $\vartheta_0 = \pi/4$.

To conclude, we study a situation in which the strong field is generated by the nanosecond front-end of the PHELIX laser [70], [$I \approx 10^{16}$ W/cm^2, $w_0 \approx 100 - 150$ μm, $\varkappa_0 \approx 1.17$ eV, $\tau \approx 20$ ns, corresponding to $\Delta\varphi \approx 5 \times 10^6 \pi$]. It is worth mentionig that the electromagnetic pulse produced by this system closely approaches to a monochromatic plane wave as the conditions $\tau \gg \varkappa_0^{-1}$ and $w_0 \gg \lambda_0$ are fulfilled simultaneously. The potential exclusion bounds which follow from this setup are valid whenever the condition $m \gg w_0^{-1} \approx 1.3$ meV is satisfied. As in the previous case, we take the probe beam with a doubled frequency $\omega_{\boldsymbol{k}} = 2\varkappa_0 = 2.34$ eV. Besides, we suppose that its intensity and waist size are much smaller than the corresponding quantities of the strong field. Assuming some achievable conditions such as $\vartheta_0 = \pi/4$, a counter propagating geometry and a sensitivity $|\psi(g,m)| \lesssim 10^{-10}$ rad, we find that the area shaded in cyan [Fig. 3] could be excluded potentially. This projected result shows that large sensitivities can be achieved, provided the number of cycles $\mathcal{N}$ is large enough to compensate for the relative smallness of the laser intensity I.

5. Conclusions

We have studied the discovery potential that modern and envisaged laser systems offer in the search for ALPs. Our investigation reveals that laser-based setups, designed to detect the hitherto unobserved QED vacuum birefringence, may provide stringent bounds on the ALP-diphoton coupling g in mass regions where the constraints resulting from experiments driven by dipole magnets are considerably less severe. Special attention has been paid to the consequences resulting from the pulse profile function, which were evaluated by solving perturbatively the system of equations describing the oscillation of photons into ALPs mediated by a generic plane-wave background. Our analysis points out that a broad sector of the parameter space of ALPs might be discarded, no matter what type of strong field profile is utilized. The precise location of the projected exclusion areas will depend, in general, on the chosen pulse profile and the CEP. However, a direct comparison between two pulses with different envelope has indicated that the outcomes resulting from the ellipticity are less sensitive to this dependence than the bounds arising from a plausible rotation of the polarization plane. Besides, we have pointed out that an appropriate choice of the CEP may optimize the ALPs search.

Acknowledgments

S. Villalba-Chávez and C. Müller gratefully acknowledge the funding by the German Research Foundation (DFG) under Grant No. MU 3149/2-1.

References

[1] R. D. Peccei and H. R. Quinn, Phys. Rev. Lett. **38**, 1440 (1977).
[2] F. Wilczek, Phys. Rev. Lett. **40**, 279 (1978).
[3] S. Weinberg, Phys. Rev. Lett. **40**, 223 (1978).
[4] M. Dine, W. Fischler and M. Srednicki, Phys. Lett. B **104**, 199 (1981).
[5] A. R. Zhitnitskii, Yad. Fiz **31**, 497 (1980); [Sov. J. Nucl. Phys. **31**, 260 (1980) (translation)].
[6] J. E. Kim, Phys. Rev. Lett. **43**, 103 (1979).
[7] M. A. Shifman, A. I. Vainshtein and V. I. Zakharov, Nucl. Phys. B **166**, 493 (1980).
[8] K. A. Meissner and H. Nicolai, Phys. Lett. B **660**, 260 (2008); [arXiv:0710.2840 [hep-th]].
[9] E. Witten, Phys. Lett. B **149**, 351 (1984).
[10] P. Svrcek and E. Witten, JHEP **06**, 051 (2006); [hep-th/0605206];
[11] O. Lebedev and S. Ramos Sanchez, Phys. Lett. B **684**, 48 (2010); [arXiv:0912.0477 [hep-ph]].
[12] M. Cicoli, M. Goodsell and A. Ringwald, JHEP **1210**, 146 (2012); [arXiv:1206.0819 [hep-th]].
[13] L. Covi, J. E. Kim and L. Roszkowski, Phys. Rev. Lett. **82**, 4180 (1999)
[14] G. G. Raffelt, J. Phys. A **40**, 6607 (2007); [arXiv:hep-ph/0611118].
[15] L. D. Duffy and K. van Bibber, New J. Phys. **11**, 105008 (2009); [arXiv:0904.3346 [hep-ph]].
[16] P. Sikivie, Int. J. Mod. Phys. A **25**, 554 (2010); [arXiv:0909.0949 [hep-ph]].
[17] H. Baer, A. D. Box and H. Summy, JHEP **1010**, 023 (2010); [arXiv:1005.2215 [hep-ph]].
[18] G. G. Raffelt, Phys. Rev. D **33**, 897 (1986).
[19] G. G. Raffelt, Ann. Rev. Nucl. Part. Sci. **49**, 163 (1999).
[20] G. G. Raffelt, Lect. Notes Phys. **741**, 51 (2008).
[21] M. Arik *et al.*, Phys. Rev. Lett. **107**, (2011) 261302.
[22] M. Arik *et al.*, Phys. Rev. Lett. **112**, (2014) 091302.
[23] E. Masso and J. Redondo, JCAP **0509**, 015 (2005).
[24] E. Masso and J. Redondo, Phys. Rev. Lett. **97**, 151802 (2006).
[25] J. Jaeckel, E. Masso, J. Redondo, A. Ringwald and F. Takahashi, *We need lab experiments to look for axion-like particles*, arXiv: hep-ph/0605313.
[26] J. Jaeckel *et al.*, Phys. Rev. D **75**, 013004 (2007).
[27] A. S. Chou *et al.* [GammeV (T-969) Collaboration], Phys. Rev. Lett. **100**, 080402 (2008).
[28] J. H. Steffen and A. Upadhye, Mod. Phys. Lett. A **24**, 2053 (2009).
[29] A. Afanasev *et al.*, Phys. Rev. Lett. **101**, 120401 (2008).
[30] P. Pugnat [OSQAR Collaboration], Phys. Rev. D **78**, 092003 (2008).
[31] C. Robilliard *et al.*, Phys. Rev. Lett. **99**, 190403 (2007).
[32] M. Fouche *et al.*, Phys. Rev. D. **78**, 032013 (2008).
[33] K. Ehret *et al.* [ALPS collaboration], Phys. Lett. B **689**, 149 (2010); [arXiv:1004.1313 [hep-ex]].
[34] R. Balou *et al.* [OSCAR collaboration], Phys. Rev. D. **92**, 092002 (2015).
[35] R. Cameron *et al.* [BFRT Collaboration], Phys. Rev. D **47**, 3707 (1993).
[36] E. Zavattini *et al.* [PVLAS Collaboration], Phys. Rev. D **77**, 032006 (2008).
[37] A. Cadne *et al.* , Eur. Phys. J. D **68**, 16 (2014); [arXiv:1302.5389 [physics.optics]].
[38] S. J. Chen *et al.* [Q&A Collaboration], Mod. Phys. Lett. A **22**, 2815 (2007); [arXiv:hep-ex/0611050].
[39] H. H. Mei *et al.* [Q&A Collaboration], Mod. Phys. Lett. A **25**, 983 (2010); [arXiv:1001.4325 [physics.ins-det]].
[40] F. Della Valle *et al.* [PVLAS Collaboration], Phys. Rev. D **90**, 092003 (2014).
[41] See: `http://www.extreme-light-infrastructure.eu`
[42] See: `http://www.xcels.iapras.ru/`
[43] A. Di Piazza, C. Müller, K. Z. Hatsagortsyan and C. H. Keitel, Rev. Mod. Phys. **84**, 1177 (2012); [arXiv:1111.3886 [hep-ph]].
[44] See: http://www.hzdr.de/db/Cms?pNid=427&pOid=35325
[45] H. P. Schlenvoigt, T. Heinzl, U. Schramm, T. E Cowan, and R. Sauerbrey, Phys. Scr. **91**, 023010 (2016).
[46] T. Heinzl, B. Leifeld, K. U. Amthor, H. Schwoerer, R. Sauerbrey, and A. Wipf, Opt. Comm. **267**, 318 (2006).
[47] V. Dinu, T. Heinzl, A. Ilderton, M. Marklund, and G. Torgrimsson, Phys. Rev. D **89**, 125003 (2014); [arXiv:1312.6419 [hep-ph]].
[48] V. Dinu, T. Heinzl, A. Ilderton, M. Marklund, and G. Torgrimsson, Phys. Rev. D **90**, 045025 (2014); [arXiv:1405.7291 [hep-ph]].
[49] B. King, and T. Heinzl, High Power Laser Science and Engineering **4**, e5 (2016); arXiv:1510.08456 [hep-ph].
[50] J. Jaeckel and A. Ringwald, Ann. Rev. Nucl. Part. Sci. **60**, 405 (2010).
[51] A. Ringwald, Phys. Dark Univ. **1**, 116 (2012); [arXiv:1210.5081 [hep-ph]].

[52] J. L. Hewett *et al.*, *Fundamental Physics at the Intensity Frontier*, The Proceedings of the 2011 workshop on Fundamental Physics at the Intensity Frontier; arXiv:1205.2671 [hep-ex].
[53] R. Essig *et al.*, *Working Group Report: New Light Weakly Coupled Particles*, arXiv:1311.0029 [hep-ph].
[54] J. T. Mendonça, Eurphys. Lett. **79**, 21001 (2007).
[55] H. Gies, Eur. Phys. J. D **55**, 311 (2009); [arXiv:0812.0668 [hep-ph]].
[56] B. Döbrich and H. Gies, JHEP **1010**, 022 (2010); [arXiv:1006.5579 [hep-ph]].
[57] S. Villalba-Chávez and A. Di Piazza, JHEP **1311**, 136 (2013); [arXiv:1307.7935 [hep-ph]].
[58] D. Tommasini, A. Ferrando, H. Michinel and M. Seco, JHEP **0911**, 043 (2009); [arXiv:0909.4663 [hep-ph]].
[59] S. Villalba-Chávez, Nucl. Phys. B **881**, 1 (2014); [arXiv:1308.4033 [hep-ph]].
[60] S. Villalba-Chávez and C. Müller, Annals Phys. **339**, 460 (2013); [arXiv:1306.6456 [hep-ph]].
[61] S. Villalba-Chávez and C. Müller, JHEP **1506**, 177 (2015); [arXiv:1412.4678 [hep-ph]].
[62] S. Villalba-Chávez and C. Müller, JHEP **1602**, 027 (2016); [arXiv:1510.00222 [hep-ph]].
[63] S. Villalba-Chávez, S. Meuren, and C. Müller, Phys. Lett. B **763**, 445 (2016); [arXiv:1608.08879 [hep-ph]].
[64] M. Born, and E. Wolf, *Principles of optics*, Pergamon Press, (1999).
[65] L. D. Landau, and E. M. Lifshitz, *Electrodynamics of continuous media, Vol. 8*, Pergamon Press, (1984).
[66] B. Marx *et al.*, Opt. Commun. **284**, 915 (2011).
[67] B. Marx *et al.*, Phys. Rev. Lett. **110**, 254801 (2013).
[68] E. Gabrielli, K. Huitu and S. Roy. Phys. Rev. D. **74**,073002 (2006); [arXiv:hep-ph/0604143].
[69] F. W. J. Olver, D. W. Lozier, R. F. Boisvert, and C. W. Clark, *NIST Handbook of Mathematical Functions*, Cambridge University Press, England, (2010).
[70] See: https://www.gsi.de/en/start/research/forschungsgebiete_und_experimente/appa_pni_gesundheit/plasma_physicsphelix/phelix.htm
[71] F. Karbstein, H. Gies, M. Reuter and M. Zepf, Phys. Rev. D **92**, 071301 (2015); [arXiv:1507.01084 [hep-ph]].